

# We are IntechOpen, the world's leading publisher of Open Access books Built by scientists, for scientists

6,600

Open access books available

178,000

International authors and editors

195M

Downloads

Our authors are among the

154

Countries delivered to

TOP 1%

most cited scientists

12.2%

Contributors from top 500 universities



WEB OF SCIENCE™

Selection of our books indexed in the Book Citation Index  
in Web of Science™ Core Collection (BKCI)

Interested in publishing with us?  
Contact [book.department@intechopen.com](mailto:book.department@intechopen.com)

Numbers displayed above are based on latest data collected.  
For more information visit [www.intechopen.com](http://www.intechopen.com)



Chapter

# Spatiotemporal Variation Analysis of Arctic Sea Ice Thickness and Volume Based on CryoSat-2 Altimetry Satellite Data

*Xubing Zhang, Ruizhi Li, Wenxi Li, Liang Zhang and Kai Wang*

## Abstract

Sea ice monitoring is helpful to the research of the Arctic channels and climate environment. Through echo signal classification, re-tracking correction, and other techniques, data from the Cryosat-2 radar altimetry satellite between 2010 and 2020 facilitated the retrieval of Arctic sea-ice thickness and volume. The study subsequently analyzed the variations in the average thickness and volume of first-year ice and multi-year ice in the Arctic sea ice over the past decade. In the past decade, the volume of sea ice in the Arctic region fluctuates slightly. The multiyear ice changed greatly in 2013, while the first-year ice shows an increased rate of both winter growth and summer ablation. The presence of uncertainties arising from the fluctuations in sea ice density values and the intricate patterns of Arctic circulation might impart subtle biases in the measurements of sea ice thickness. However, the sea ice freeboard and thickness data inverted based on the Cryosat-2 data were validated by the data obtained through the Operation Ice Bridge (OIB), and the validation results indicated that they are correspondent.

**Keywords:** sea ice, Cryosat-2, the Arctic, thickness, volume

## 1. Introduction

As an indicator of the Arctic climate, the sea ice is affected by the climate change and reacts to global climate. It is an important indicator of global climate change research and a window to understanding the current situation and change trend of the Arctic environment. For a long time, limited by the harsh natural environment of the Arctic region, the Arctic sea ice observation is high cost and low efficiency. Therefore, it is difficult to realize the large-scale, multi-scale, and long-time series monitoring. With the rapid development of remote sensing technology, satellite altimetry has become an effective method to continuously obtain the accurate global thickness information on the sea ice [1]. The Earth Explorer Opportunity Mission-2 (CryoSat-2) satellite which launched in April 2010, with full coverage of the Arctic region and a

centimeter-level precision [2], could meet the need for long-term monitoring of the sea ice thickness.

At the same time, the theoretical method of the altimetry satellite inversion of the sea ice thickness has also attracted the attention of many researchers. In 2003, the sea ice thickness in the  $40^{\circ}\text{N} \sim 81.5^{\circ}\text{N}$  range was retrieved by Peacock, Laxon et al. based on the Earth Resources Satellite-1 altimetry satellite [3, 4]. As mentioned in the articles [3, 4], the sea ice was distinguished from the water according to the pulse peaks and backscattering coefficients of the radar echo signals. After that, the echo signals are corrected by the re-tracking algorithm to calculate the elevation of the sub-satellite point and obtain the elevation difference between the sea ice and the surrounding seawater namely sea ice freeboard. Then, the sea ice thickness is estimated based on the static equilibrium state of the sea ice, and some parameters such as snow density and snow depth as well. Currently, the echo signals classification [5–8], re-tracking correction algorithm [9–12], and sea ice thickness inversion model parameters [13–16] have become hot issues in sea ice thickness monitoring.

To study the changes in the Arctic sea ice thickness between 2010 and 2019, this paper selects the following data such as the CryoSat-2 data with high accuracy and full coverage, the MASAM2 sea ice density product with daily update of the 4 km resolution grid, the OSI SAF (Ocean and Sea Ice Satellite Application Facility) daily update product of the sea ice type with 10 km resolution grids, the UCL13 MSS (Mean Sea Surface model of the University College London 2013) and the ice snow thickness data with the 24 km resolution grids of daily update produced by the Canadian Meteorological Center. With the above data, this paper analyzes the variation characteristics of the sea ice thickness in recent years, which could provide the data basis for the change trend research of the large-scale sea ice thickness in the Arctic region.

## **2. Sea ice thickness inversion data**

### **2.1 Cryosat-2 altimetry satellite data**

CryoSat-2 was launched by the ESA on April 8, 2010. The Synthetic Aperture Radar Altimeter (SIRAL), carried by CryoSat-2, includes three modes of operation: Low-Resolution Measurement Mode (LRM), Synthetic Aperture Radar Mode (SAR), and Synthetic Aperture Radar Interferometry Mode (SARIn). The LRM model is primarily used to make measurements of continental ice caps and the vast majority of the Earth's ice-free ocean and land areas. The SAR model measures mainly the sea ice and some ocean basins and coastal areas. The SARIn model measures mainly the ice cap, mountain glaciers, ground-transfer currents, hydrographic basins, and the coastal zone regions. In this paper, the L1B data of the SAR model and SARIn model are used to estimate the Arctic Sea ice thickness before September 2014, and the L1B data of the SAR model is used to retrieve the whole Arctic Sea ice thickness after this time point.

### **2.2 Sea ice density data**

The sea ice density product is used to classify the CryoSat-2 radar satellite echo signal waveforms. We use the SSM/I\_SSMIS dataset provided by the National Snow and Ice Data Center (NSIDC) to obtain sea ice density data from October 2010 to March 2012, which provides daily and monthly updates of 25 km gridded sea ice

density data [17, 18]. After October 2012, the MASAM2 (MASIE-AMSR2) dataset provided by NSIDC was used. Compared with the AMSR2, the MASAM2 data are less affected by the weather, have higher accuracy and resolution, and are more accurate in calculating the sea ice density during sea ice melt. The visualization of the MASAM2 data is shown in **Figure 1**.

### 2.3 Sea ice type data

The sea ice type data could assist in calculating the sea ice thickness. We use the Ocean and Sea Ice (OSI SAF) dataset produced by the Norwegian Meteorological Service's Ocean and Sea Ice Satellite Application Facility (OSSAF), which is a daily updated 10 km grid sea ice type product from 2005 to the present [19]. A schematic diagram of the sea ice type data visualized from the OSI SAF for March and October 2018 is shown in **Figure 2**.

### 2.4 Sea ice snow thickness data

As the input parameter of the sea ice static equilibrium model, the sea ice snow thickness data are directly related to the accuracy of the sea ice thickness calculation

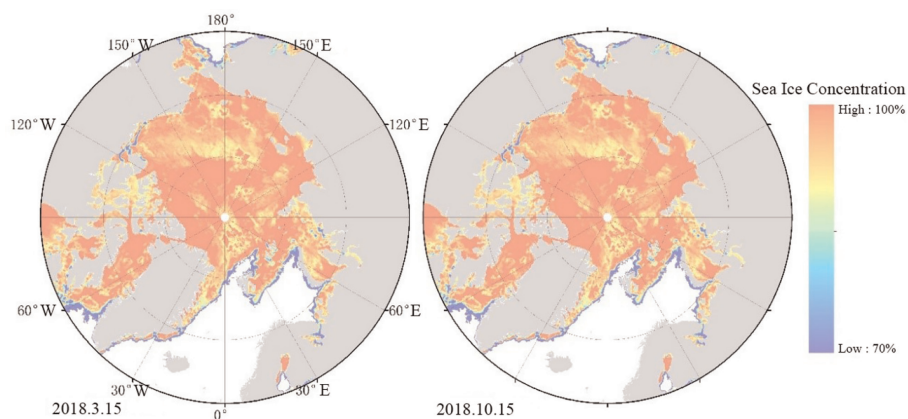


**Figure 1.**  
*The MASAM2 sea ice density data.*

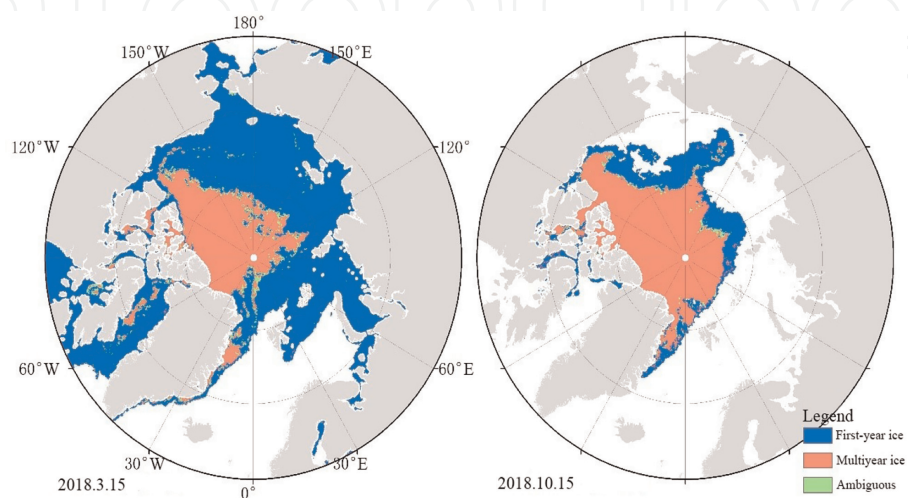


**Figure 2.**  
*Schematic diagram of the OSI SAF sea ice type products in March and October 2018.*

results. The daily updated snow thickness data from the Canada Meteorological Centre (CMC), is a dataset based on the snow depth data provided by the World Meteorological Organization Information System (WMOIS) and daily snow thickness measurements in the field [20]. A schematic of the monthly average snow thickness data for March and October 2018 for this dataset is shown in **Figure 3**.

## 2.5 The operation ice bridge data

The Operation IceBridge (OIB) science data are used to validate the results of the sea ice thickness inversion process. IceBridge L4 sea ice freeboard height, snow depth, and ice thickness data (IDCSI4, IceBridge L4 Sea Ice Freeboard, Snow Depth, and Ice Thickness) are used to validate the sea ice freeboard and thickness inversion results of this study [21, 22]. The March 2013 OIB flight path is shown in **Figure 4**.

## 2.6 Arctic mean sea surface data

The Mean Sea Surface in the Arctic region is one of the parameters used for the sea ice freeboard estimation. We use the UCL13 mean sea surface model produced by

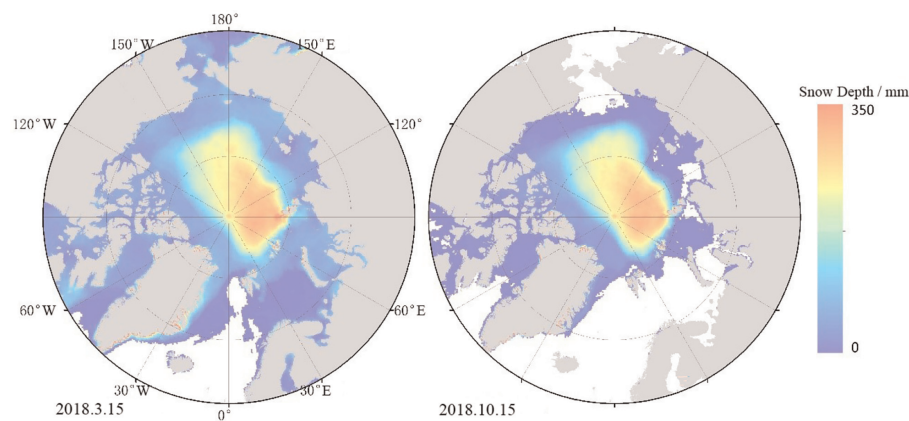


**Figure 3.** Schematic of the Canadian Meteorological Centre snow thickness products in March and October 2018.

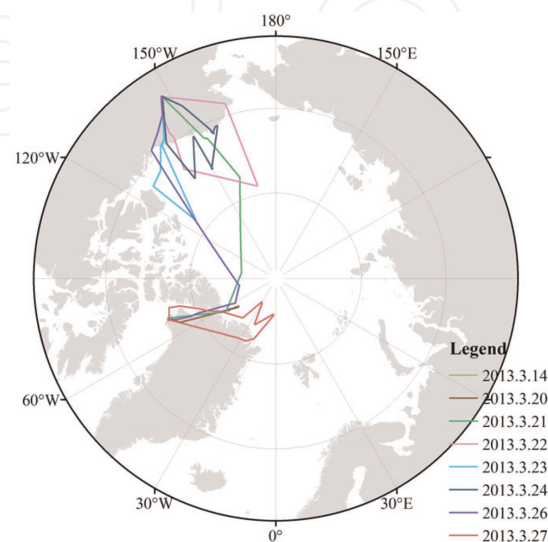


**Figure 4.** Schematic diagram of the March 2013 OIB flight path.

University College London (UK) in 2013. Because previous mean sea surface models of the Arctic lacked satellite data north of 81.5°N, the UCL13 is more accurate over the entire Arctic region [23–25].

### 3. Sea ice thickness inversion

The thickness and volume of the sea ice in the Arctic region are estimated in this paper by using L1b level data from the Cryosat-2 radar altimetry satellite, and the main steps are illustrated in **Figure 5**. First, the echo signal data in the Arctic sea region are denoised. Then, the echo signal classification and re-tracking correction are performed, and the sub-satellite point elevation is calculated. Finally, the sea ice thickness is calculated based on the sea ice static equilibrium model, supplemented by the snow depth and the sea ice density data.

#### 3.1 Data preprocessing

The satellite altimeter transmits and receives the reflected pulse signals to the sub-satellite point, and the distance from the satellite altimeter to the sub-satellite point is obtained by calculating the time difference between the transmitted and received pulse signals [26–28]. Where the echo signal waveform reflected from the sub-satellite point is recorded in the CryoSat-2 satellite L1b data, the shape of which is shown in **Figure 6**. The echo signal information needs to be pre-processed to reduce the background radiation, the instrument noise, or the waveform anomalies. The satellite data in the region north of 60°N latitude is also screened to remove waveforms with missing or mutilated information.

#### 3.2 Echo signal classification

The pulse-peakiness (PP) and the pulse standard deviation so-called stack standard deviation (SSD) are used to distinguish between the sea ice and the seawater in this paper [6]. The pulse peak value is used to describe the shape of the echo signal, and

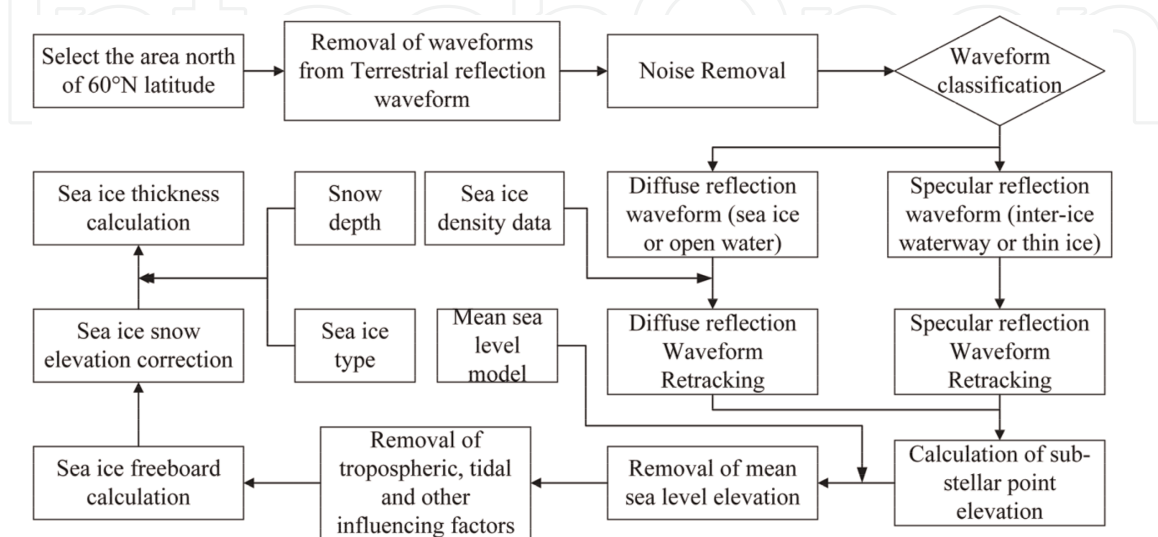


**Figure 5.** Inversion process of the sea ice thickness.

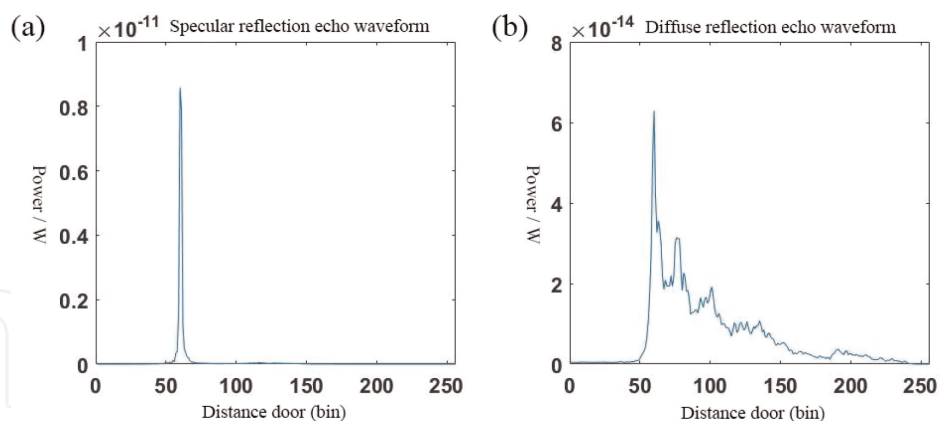


**Figure 6.** Cryosat-2 measurement waveform. (a) is the specular echo; (b) is the diffuse echo.

the larger the value is, the peak exists in the waveform. The pulse standard deviation is the standard deviation of the scattering direction of the echo signal. And the larger the value is, the more dispersed the echo signal reflected from the surface is, conversely, the reflection direction of the echo signal is concentrated. Pulse standard deviation values are provided in the L1b file, and the  $PP$  value is calculated using the following equation:

$$PP = \frac{P_{max}}{P_{mean}} \quad (1)$$

Where  $PP$  is the pulse-peakiness,  $P_{max}$  is the maximum power in the echo signal, and  $P_{mean}$  is the average power in the echo signal. Specular echoes occur when the radar pulses are reflected from a smooth, mirror-like surface such as the sea ice leads or very thin ice (**Figure 6a**). Diffuse echoes occur when the radar pluses are reflected from a rougher surface such as an ice floe or the open ocean (**Figure 6b**).

Specular echoes are defined as those with a pulse-peakiness greater than 18 and the SSD less than 6.29 for SAR mode echoes or the SSD less than 4.62 for SARIn mode echoes. Diffuse echoes are those with a pulse-peakiness less than 9 and the SSD greater than 6.29 for SAR mode echoes or the SSD greater than 4.62 for SARIn mode echoes [6]. Subsequently, it is necessary to distinguish the echoes of the sea ice from the echoes of the ocean, as both are classified as diffuse reflection waveforms. Additionally, the sea ice concentration products MASIE-AMSR2 used in this paper only recorded the regions with sea ice concentration above 70%. We thereby define the sea ice regions as those with a sea ice concentration greater than 70%, or else, the diffuse echoes are not trusted to come from either sea ice or open ocean and are removed from the processing.

### 3.3 Echo signal re-tracking correction

The distance between the satellite altimeter and the sub-satellite point is calculated by the time interval between the satellite altimeter transmitting pulse signal and receiving the echo signal reflected by the ground object. Generally, the time tracking point of the transmitting signal has been set on the satellite. Similarly, the time tracking point of the echo signal is pre-set at the midpoint of the waveform sampling window. However, the actual tracking point would always be offset from the original

set tracking point, but the round-trip time of the pulse signals is still calculated according to the positions of the original set tracking points. That it is necessary to correct the distance differences between the actual tracking points and the preset tracking points to obtain high-precision height measurement values [29]. In this paper, a threshold first maximum re-tracker (TFMRA) is adopted, which is based on the empirical estimation of statistical [15]. The flow chart is shown in **Figure 7**. The main formulas are shown in Eqs. (2)–(5):

$$P_{noise} = \frac{1}{noise} \sum_i^{noise} P_i \quad (2)$$

$$A = \max((P_n)_{First}), n = 1, 2, 3, \dots, N \quad (3)$$

$$(A > 0.15 + P_{noise})$$

$$T_h = P_{noise} + q \times (A - P_{noise}) \quad (4)$$

$$Re = G_{k-1} + \frac{T_h - P_{k-1}}{P_k - P_{k-1}} \quad (5)$$

where *noise* is the number of the range bins, and the value in the Cryosat-2 echo signal is generally 6.  $P_{noise}$  is the noise value of echo waveform. The average value of the echo power corresponding to the first six range bins is taken as the noise value  $P_{noise}$ .  $P_i$  is the echo power corresponding to the range bin  $i$ .  $A$  is the first peak of the echo waveform, and it needs to be larger than the sum of 0.15 and the value of  $P_{noise}$ .  $P_n$  is the power value of the normalized echo waveform.  $n$  is the number of the range bins, and the total number of the range bins is 256 in the SAR mode, and 1024 in the SARIn mode.  $q$  is the proportional coefficient namely the threshold value.  $T_h$  is the power value of the re-tracking point.  $Re$  is the range bin number obtained after re-tracking

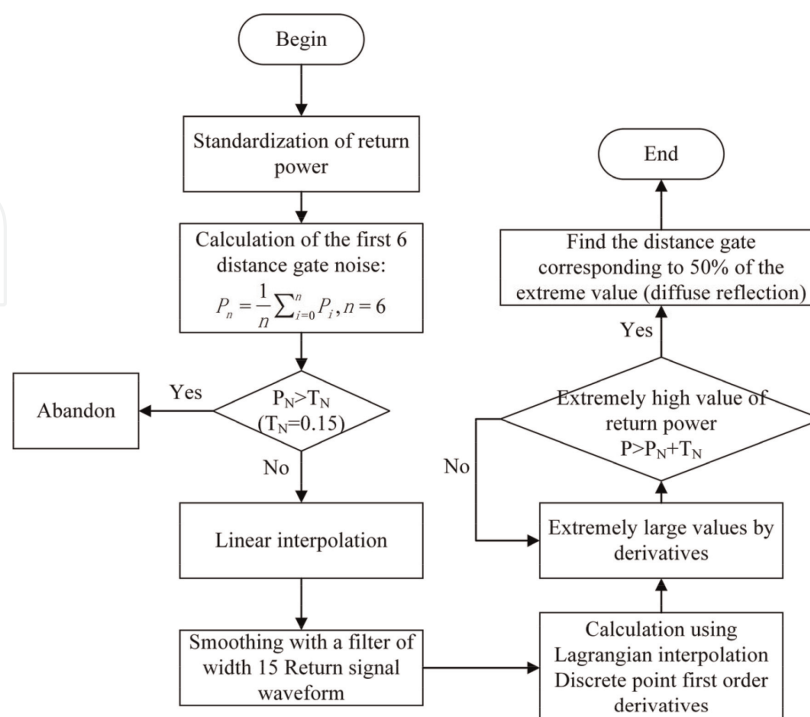


**Figure 7.**  
 Flow chart of TFMRA.



correction, and if it is between two range bins, it would be calculated by linear interpolation.  $G_{k-1}$  is the previous range bin corresponding to  $Re$ .

### 3.4 Sea ice freeboard inversion and verification

After re-tracking correction, the sea ice and seawater elevation could be calculated, and then the sea ice freeboard value is obtained. **Figure 8** shows the schematic diagram. The orbit elevation  $h_{cs}$  of the altimetry satellite is known and stored in the L1b file. First, the distance  $H$  between the sub-satellite point and the altimetry satellite is calculated by the round-trip time of the radar pulse. The difference between  $h_{cs}$  and  $H$  is the elevation value of the sub-satellite point under the reference of the WGS84 ellipsoid. Then the sea ice freeboard is calculated according to the elevation difference between the sea ice and the sea ice leads. Although some experiments have shown that the scattering layer of the radar pulse at the ice-snow interface of the sea ice with snow cover varies with the increase in temperature [30]. However, the variation of the scattering layer has little effect on the results in the annual sea ice observation [31]. Therefore, we assume that the radar pulses are scattered at the ice-snow interface, and the formulas are shown in Eqs. (6)–(8):

$$h_f = h_{CS} - h_{ssh} - H - C_G \quad (6)$$

$$H = \frac{ct_n}{2} + C_R \quad (7)$$

$$C_R = (b_0 - b_n)\Delta_b \quad (8)$$

Where  $h_f$  is the freeboard of the sea ice, representing the height of sea ice above sea level.  $H_{ssh}$  is the elevation of the local sea level. And this paper refers to the elevation value of the Arctic sea surface model UCL13.  $C_G$  is the influence of various factors in the atmosphere on a radar range, such as dry troposphere, wet troposphere, ionosphere, ocean tide, geocentric polar tide, and so on.  $C$  is the speed of light.  $t_n$  is the time in which the radar pulse is transmitted from the satellite and reflected by the surface of the sub-satellite point, and then received by the satellite.  $C_R$  is the re-tracking correction value.  $b_0$  is the number of the range bin located in the middle,

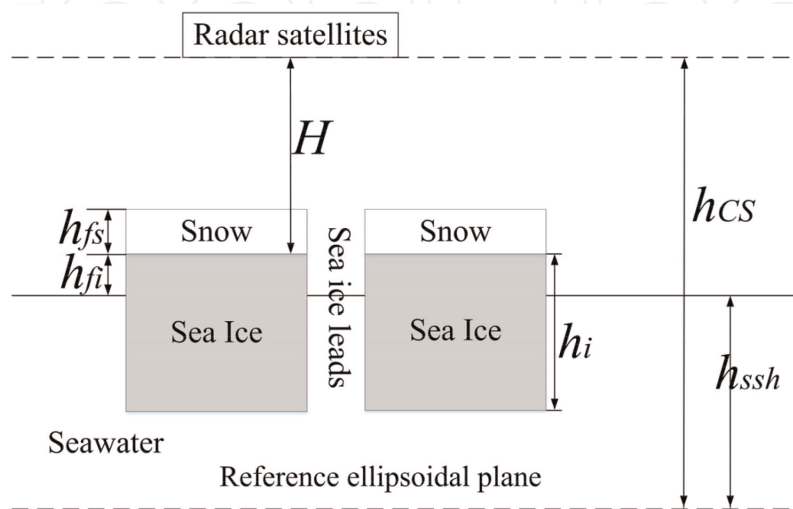


**Figure 8.** Schematic diagram of sea ice altimetry.

which is 128 in SAR mode and 512 in SARIn mode.  $b_n$  is the number of the bin determined by waveform re-tracking and  $\Delta_b$  is the bin width (0.2342 m).

Because the electromagnetic waves will travel slower when they move into the snow layer, it will cause errors in calculating the freeboard. It is necessary to modify the calculation of the sea ice freeboard. The corrected sea ice freeboard is shown in Eq. (9) [31]:

$$f_c = f_i + h_s \left( \frac{c_v}{c_s} - 1 \right) \quad (9)$$

where  $f_c$  is the corrected sea ice freeboard.  $f_i$  is the original sea ice freeboard.  $h_s$  is the snow depth.  $c_v$  is the speed of light propagation in a vacuum ( $3 \times 10^8$  m/s). And  $c_s$  is the speed of light propagation in the snow ( $2.4 \times 10^8$  m/s). Therefore, the corrected freeboard is simply expressed as:

$$f_c = f_i + 0.25 \times h_s \quad (10)$$

To comprehensively evaluate the effect of the echo signal correction based on TFMRA, the sea ice freeboard values, which were inverted by TFMRA based on the different threshold  $q$  Eq. (4) of the sea ice, are compared with that of the airborne OIB data. The verification time selected is March 2013, during which the flight missions of the airborne OIB data are only carried out within seven days from March 20 to 24, and 26 to 27. The flight route was in the sea area of northern Canada. Cryosat-2 satellite data from March 18 to 29 are selected for inversion verification. The horizontal spatial resolution of Cryosat-2 is about 300 meters, while that of OIB data is close to 1 meter, and then the Cryosat-2 data points are sparse and the OIB data points are dense. To compare the two data, a 5 km resolution grid is made based on the OIB data. The average value of data points in the grid is used to represent the value of the grid. The grid containing both Cryosat-2 and OIB data points was selected for comparison. A total of 1172 grids meet the requirements. **Figure 9** shows the freeboard diagram of the sea ice measured by airborne OIB.

The statistics of the survey points in the 1172 grids are shown in **Table 1**. The number of the altimetry points of the Cryosat-2 in the grid is far less than that of the

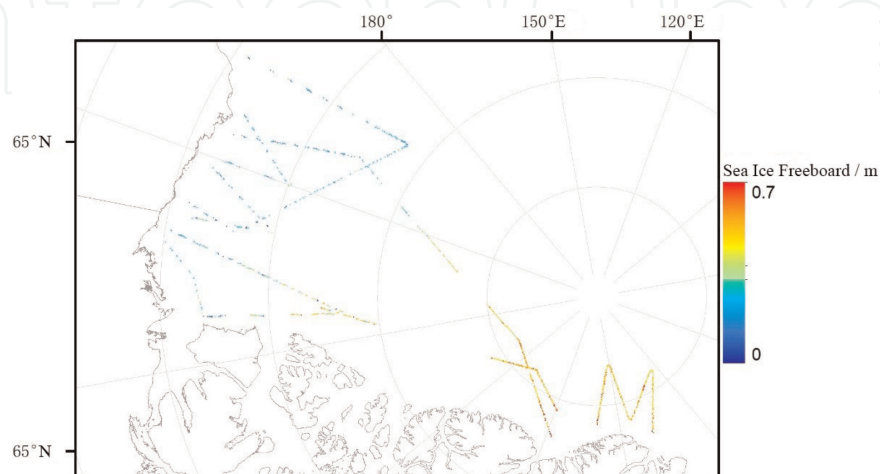


**Figure 9.** Schematic diagram of sea ice freeboard measured by airborne OIB in March 2013 (Using WGS 1984 North Pole LAEA Atlantic projection coordinate system).

	Total number	Mean value	Maximum value	Minimum	Median
OIB high points	78,696	67.20	155	1	69
Cryosat-2 high points	12,034	10.28	42	1	8

**Table 1.**  
Inversion of the number of high points in 1172 grids.

airborne OIB, and the altimetry points of both data are not evenly distributed in the grids. Inevitably, there are some errors between the measured values of the Cryosat-2 data and that of the airborne OIB. Comparing the altimetry data of Cryosat-2 within 10 days and the measured data of the OIB within 7 days. Because of the inconsistent timing of the acquisition of the two types of data, it is possible that the sea ice thickness changed during this period, resulting in some errors between the Cryosat-2 and the OIB data.

Calculating the sea ice freeboard requires the local sea level elevation. We use UCL13 mean sea level elevation model produced by the University of London to obtain the sea level elevation of sea ice. The threshold  $q$  Eq. (4) is significant to the results of the TFMRA. Therefore, the threshold  $q$  of the sea ice was set to 0.5, 0.6, 0.7, and 0.8 to correct the sea ice echo signal by TFMRA, respectively. The sea ice freeboard values are calculated based on the UCL13 sea level average elevation model and the Canadian snow data set, and the results compared with the OIB measurements are shown in **Table 2**.

The scatter plots based on the airborne OIB measurements and the inversion freeboard values on different thresholds are shown in **Figure 10**. Every scatter point denotes the inversion freeboard mean value and the OIB measurement mean value of the altimetry points in the same grid abovementioned. The scatter plot shows the difference in the number and distribution of the inversion freeboard values and OIB measurements in the grids. Ideally, the more points are concentrated in the line of  $y = x$ , the closer the inversion freeboard values are to the OIB measurements, which is more consistent with the actual situation.

As shown in **Figure 10a**, the scatter points are concentrated in the lower right area, which means that the inversion freeboard values are generally larger than the OIB measurements, and the largest deviation is 18.7 cm, when the threshold is set to 0.5. As shown in **Figure 10c**, the scatter points are relatively evenly distributed on both sides of the  $y = x$  line, which means that the inversion freeboard values are generally

	OIB data/m	TFMRA-50% threshold value/m	TFMRA-60% threshold value/m	TFMRA-70% threshold value/m	TFMRA-80% threshold value/m
Mean value	0.380	0.567	0.463	0.361	0.263
Mean difference	/	0.187	0.083	-0.019	-0.117
RMSE	/	0.257	0.198	0.187	0.222
Correlation coefficient	/	0.512	0.463	0.427	0.385

The significance of “/” is that values are missing.

**Table 2.**  
Comparison of airborne OIB freeboards and sea ice freeboards based on different threshold values of the sea ice according to TFMRA.

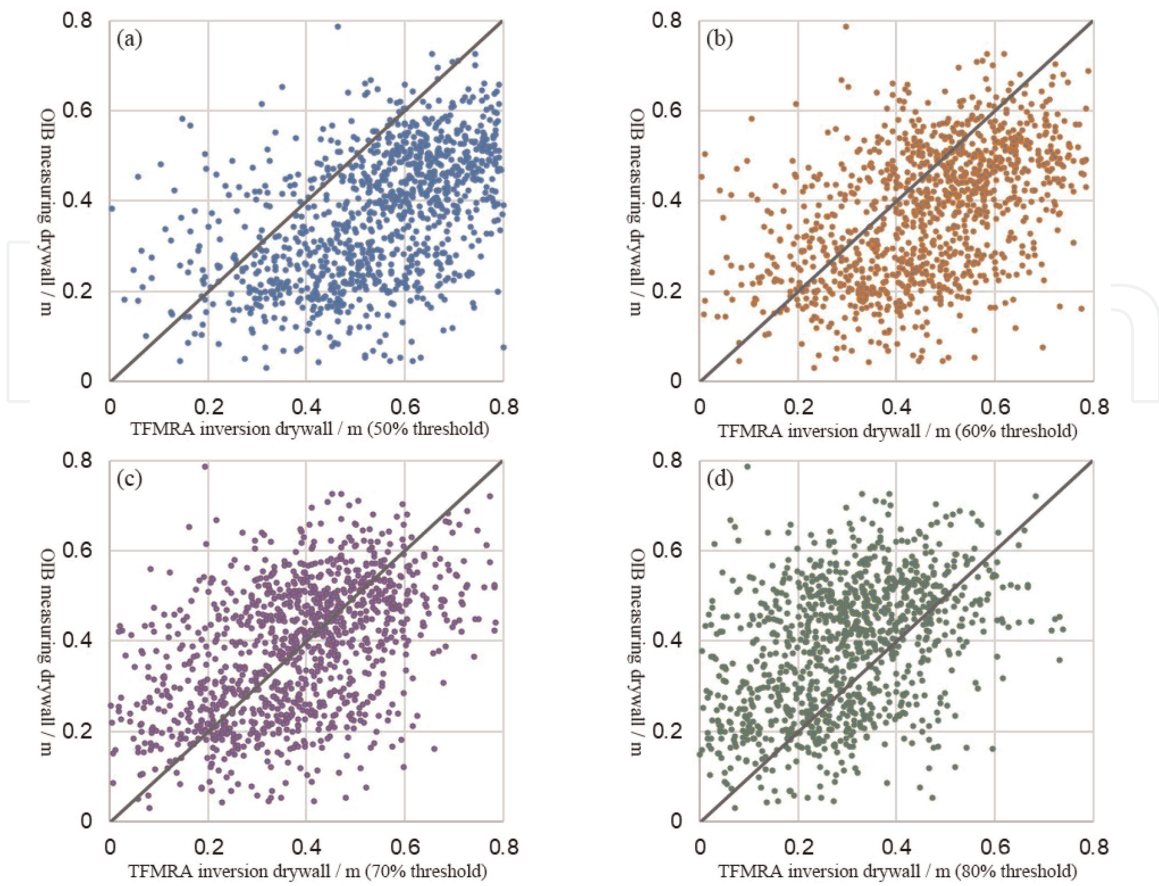


**Figure 10.** Freeboard scatters point inversion based on different thresholds of TFMRA and OIB. (a) 50% threshold inversion; (b) 60% threshold inversion; (c) 70% threshold inversion; (d) 80% threshold inversion.

closer to the OIB measurements, and the average deviation is 1.9 cm, when the threshold is set to 0.7. Overall, compared the four plots of **Figure 10** the freeboard inversion results are the most consistent with the actual situation when the threshold is set to 0.7.

### 3.5 Sea ice thickness inversion and verification

According to the actual situation of the sea ice in the Arctic ocean, it is assumed that the sea ice covered with snow is in equilibrium with the seawater. The sea ice thickness could be calculated by the static equilibrium model [3], as shown in Eq. (11):

$$h_i = \frac{f_c \rho_w + h_s \rho_s}{\rho_w - \rho_i} \quad (11)$$

where  $h_i$  is the sea ice thickness,  $f_c$  is the sea ice freeboard, and  $\rho_w$  is the density of the seawater. In this paper, the seawater density is  $1023.9 \text{ kg/m}^3$ .  $h_s$  is the snow thickness on the sea ice, referring to the snow thickness data of the Canada Meteorological Center.  $\rho_s$  is the snow density on the sea ice, referring to Spreen [32], being  $330 \text{ kg/m}^3$ .  $\rho_i$  is the sea ice density, which is  $882.0 \text{ kg/m}^3$  for multi-year ice density and  $916.7 \text{ kg/m}^3$  for first-year ice density, referring to Alexandrov [33].

In most cases, the hydrostatic equilibrium model is applicable to the calculation of sea ice thickness. However, sometimes, as the thinner sea ice is pressed by the thick

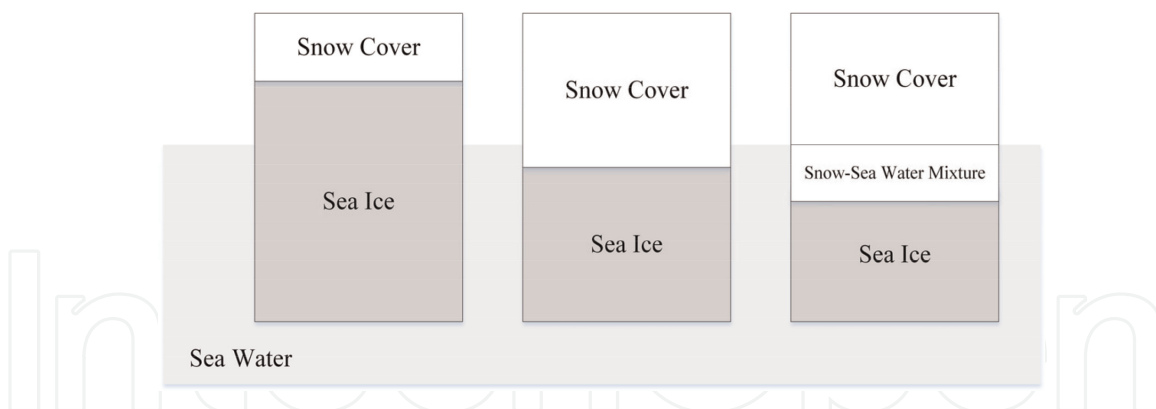


**Figure 11.** Static equilibrium model in various cases (from left to right, the freeboard value is positive, zero, and negative).

snow and fluctuates up and down by the wave influence, and the seawater may penetrate the sea ice snow and form a snow-water mixture (**Figure 11**) [34, 35]. Under these circumstances, the sea ice freeboard values measured by the satellite altimeter may be zero or negative.

When the freeboard of sea ice is zero or negative, the properties of the snow-water mixture layer are very different from those of the sea ice and the snow cover. Therefore, when the snow cover, snow water mixture, and the sea ice are in equilibrium in the seawater, the calculation formula of the sea ice thickness is shown in Eqs. (12) and (13) [36]:

$$h_i = \frac{\rho_{slh} - \rho_w}{\rho_w - \rho_i} \times h_{slh} + \frac{\rho_s}{\rho_w - \rho_i} \times h_s \quad (12)$$

$$h_{slh} = -h_f \quad (13)$$

where  $h_i$ ,  $h_s$ ,  $\rho_w$ ,  $\rho_s$  and  $\rho_i$  are the same as the Eq. (11).  $h_f$  is the freeboard height of sea ice,  $h_{slh}$  is the thickness of the snow water mixture, and  $\rho_{slh}$  is the density of the snow water mixture. The thickness of the snow-water mixture layer is equal to the absolute value of the sea ice freeboard, and its density is  $940 \text{ kg/m}^3$  [37].

To verify the availability of the inversion results of the sea ice thickness, the inversion results were compared with the airborne OIB data. The abovementioned 5 km resolution grids based on OIB data are adopted here. The grids containing Cryosat-2 and OIB data points were selected for verification. A total of 1025 grids met the requirements. The sea ice thicknesses measured by the airborne OIB are shown in **Figure 12**. The Canadian snow data product and UCL04 snow thickness model are used to calculate the sea ice thickness, and the results are compared with the airborne OIB measurement data, respectively as shown in **Table 3**.

As shown in **Figure 13**, at sea ice thickness of less than 1 m, there is a large difference between the calculated sea ice thicknesses of the Canadian snow data product and the UCL04 snow thickness model. The points in **Figure 13a** are scattered, while the points in **Figure 13b** are closer to the  $x = 1$  line. Can be introduced on sea ice thinner than 1 meter, UCL04 have larger thicknesses of the snow on the sea ice than that of the Canadian snow data.

When the reversion values of the sea ice thicknesses are greater than 1 m, the points in **Figure 13a** and **b** are distributed consistently and concentrated in the lower right region of the  $y = x$  straight line, indicating that the Canadian snow data product and the UCL04 have almost the consistent snow thicknesses.

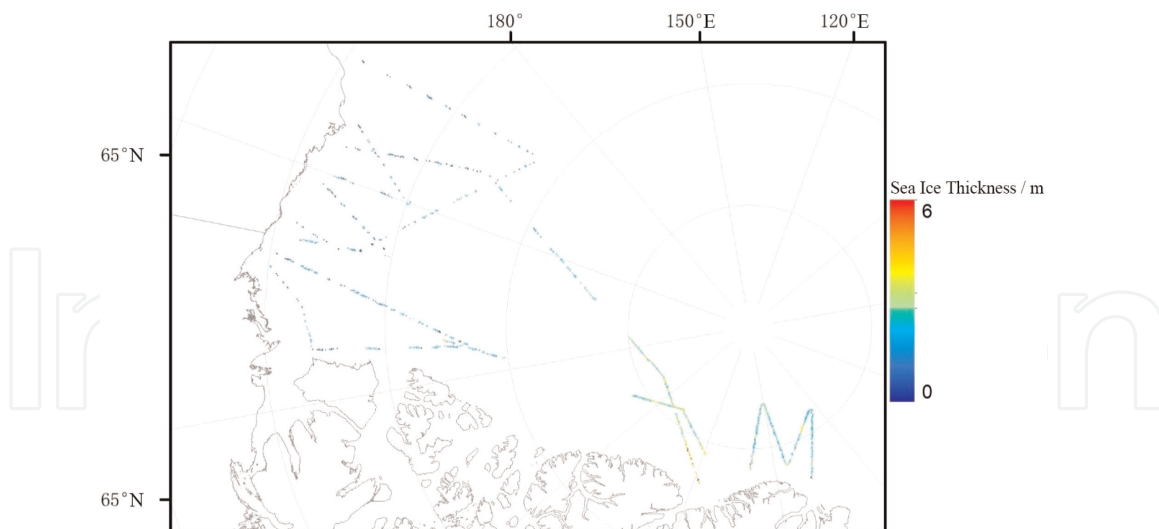


**Figure 12.**  
 The sea ice thicknesses were measured by airborne OIB in March 2013 (Using WGS 1984 North Pole LAEA Atlantic projection coordinate system).

	Thickness measured by OIB / m	Sea ice thickness calculated by combining Canadian snow cover thickness/m	Sea ice thickness calculated by combining UCL04 snow cover thickness/m
Mean value	2.239	2.764	2.961
Mean difference	/	0.525	0.722
RMSE	/	0.882	1.085
Correlation coefficient	/	0.756	0.675

The significance of “/” is that values are missing.

**Table 3.**  
 Comparison of the inversion values of the sea ice thicknesses based on different snow products and the sea ice thickness measured by airborne OIB.

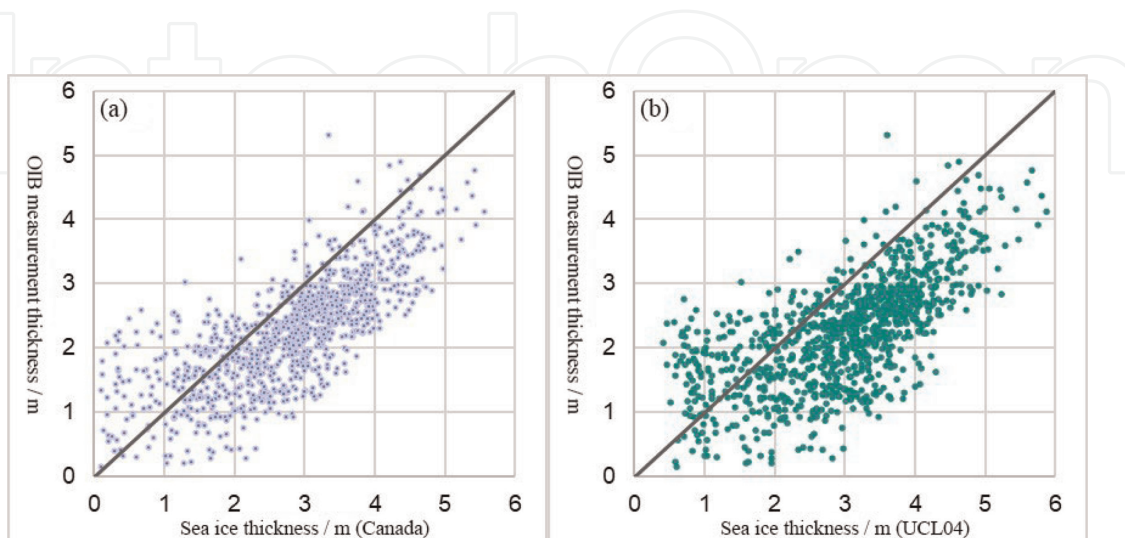


**Figure 13.**  
 Scatter plot of inversion values of the sea ice thicknesses based on different snow products and the sea ice thicknesses measured by OIB.

Combined with **Table 3**, the average reversion values of the sea ice thicknesses based on the Canadian snow data are closer and more correlated to the airborne OIB measurements. The slightly larger reversion values than the OIB measurements may be due to the low signal-to-noise ratio of the snow radar echo signal in the ice ridge region used in the OIB, which resulted in the underestimation of the actual sea ice thickness by the airborne OIB [38]. In summary, the Canadian snow data products are largely reflective of Arctic Sea ice thickness variability.

In summary, compared to the sea ice inversion values based on the UCL04, the inversion values based on the Canadian snow data have a smaller average difference and a higher correlation coefficient with the OIB measurements, therefore the Canadian snow data product was adopted here to invert the sea ice thickness.

## 4. Sea ice thickness and volume change analysis in the arctic

### 4.1 Analysis of Arctic Sea ice thickness variation

According to the above steps, the Arctic sea ice thickness data are inverted based on the Cryosat-2 data. It is notable that since the limitation of the sea ice concentration products MASIE-AMSR2 (Section 3.2) the inversion sea ice thickness data are distributed only in the regions where the sea ice concentration is greater than 70%. And then the inversion sea ice thickness data are divided using a 5 km resolution grid north of 60°N (Stereographic North Pole for projection). The sea ice thickness of each grid is represented by the average of the sea ice thickness of the data points within the grid, and if there are less than 5 available altimetry points in this grid, the average of the sea ice thicknesses of the surrounding 8 grids would be taken as the sea ice thickness of this grid. Studies show that the annual sea ice coverage area was greatest in March, and as temperatures rose in April, the sea ice continued to melt and the sea ice coverage area and thickness decreased to the lowest point in October [39]. Therefore, to highlight the change of sea ice, the sea ice thicknesses in March and October are inverted and compared in this paper.

**Figures 14** and **15** depict the schematic distribution of the sea ice thickness in October and March in the last decade. The sea ice coverage is almost all in the core area of the Arctic Ocean. In October, there is almost no sea ice grid in the Chukchi, Beaufort, and the Barents Seas, and only a few in the East Siberian and the Kara Seas. **Figure 16** depicts the grids of the different sea ice thicknesses, where the horizontal coordinate is the thickness of the sea ice, the vertical coordinate is the number of grids, and the different colored polygonal lines represent different years.

We can see that, in October, the sea ice is mostly 1–2 meters thick, while in March, it is around 2 meters thick.

According to **Figure 16a**, sea ice in October 2016 exceeded subsequent years in terms of the grid amount and the thickness, which showed a decreasing trend after 2016. In particular, the grid amount of the sea ice thickness being no less than 2 m was the lowest in October 2011, and the grid amount of the sea ice thickness is less than 2 m was lowest in October 2018. **Figure 16b** shows that the grid amount of the sea ice thickness arrives to the highest peak when the sea ice thicknesses are around 2 m in March of each year. Furthermore, the highest peak grid amount was the largest in March 2020 and lowest in March 2018.

The average sea ice thicknesses in March and October from 2010 to 2020 are shown in **Figure 17**. There are large fluctuations in the average sea ice thickness [40].

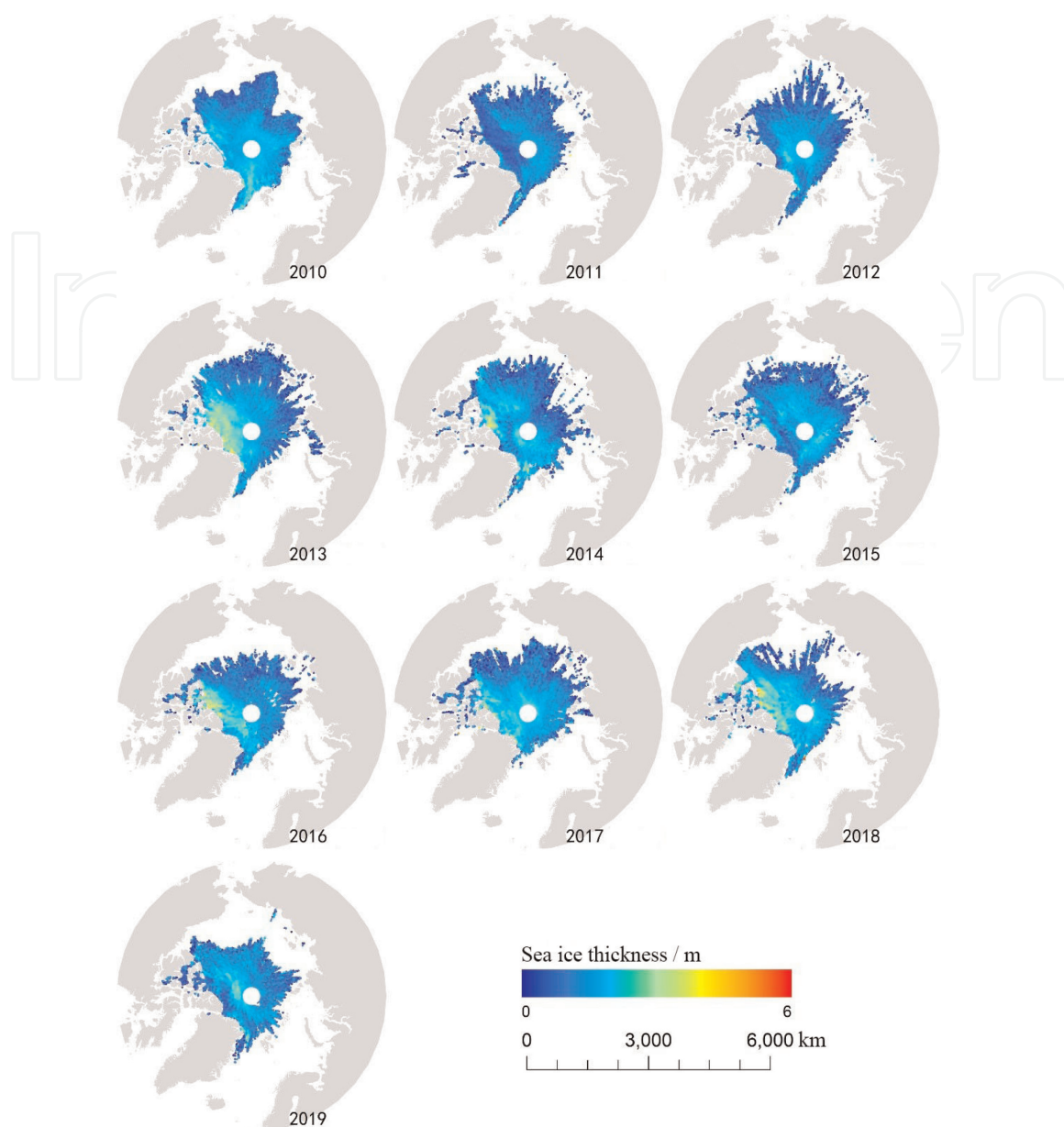


**Figure 14.**  
*Sea ice thickness distribution in October from 2010 to 2019.*

In October 2011, compared to October 2010 the average sea ice thickness decreased by 26.13%, or 0.38 m, which is also the largest decrease in the average sea ice thickness in nine years. In October 2013, compared to October 2012 the average sea ice thickness showed a significant increase of 22.88% or 0.27 meters. In March 2014, compared to March 2013 the average sea ice thickness increased by 15.55%, or 0.29 m. It reached the maximum value of the average sea ice thickness in the past nine years. In March and October 2015, compared to October 2014 the average sea ice thickness decreased by 2.29% and 7.75%, respectively. In October 2016, the average sea ice thickness showed a significant increase of 12.57%. And in March and October 2017, the average sea ice thickness changed very slightly, with the changes both within 1%. In October 2018, the average sea ice thickness showed a small increase with 10.71% growth. In March 2019, the average sea ice thickness increased by 5.4%. In March 2020, the average sea ice thickness decreased by 7.82%. The average sea ice thickness showed a significant increase in March 2014 and a small decreasing trend in the rest of the



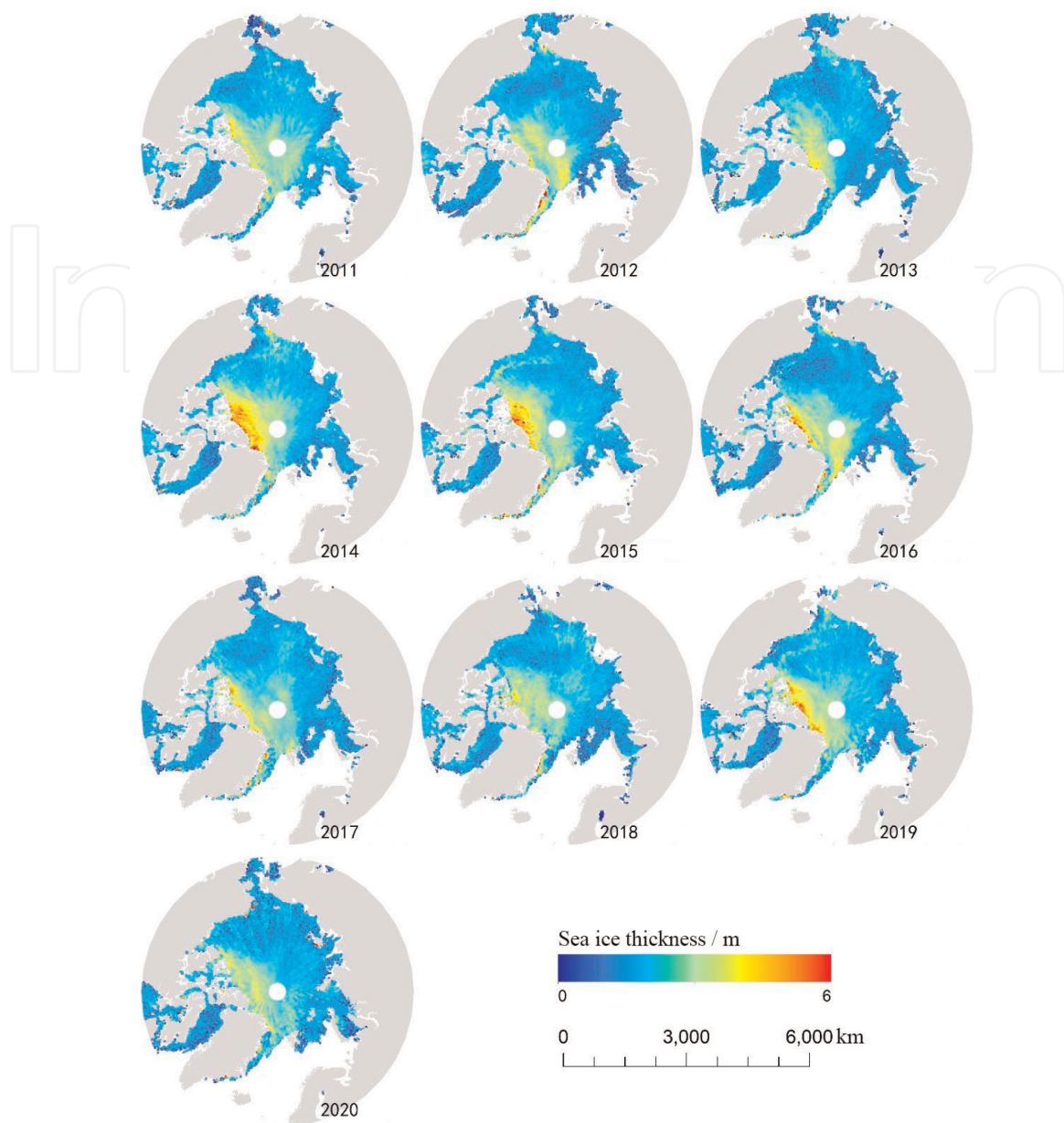


**Figure 15.**  
Sea ice thickness distribution in March from 2011 to 2020.

years, with an average annual change rate of  $-0.51\%$ . Overall, the variation of the average sea ice thickness in March is relatively stable over the years.

October is the end of autumn in the Arctic region, and the Arctic will enter a long winter in November. After the melting of the peripheral sea ice in summer, only the sea ice remains in the core of the Arctic region. The average sea ice thickness change in October is consistent with the trend of the multiyear ice volume change. Before 2013, the average sea ice thickness was highly variable. After 2013, the average sea ice thickness decreased slightly in 2015 and increased slightly in 2018. The annual mean sea ice thickness decreased by  $0.012$  m in October 2019 compared to October 2010, with an average change of  $0.18\%$ . In general, there are small fluctuations in the average thickness change of sea ice in October over the years, and the overall trend is stable. This is consistent with the findings of Hiroshi Sumata et al. [41] and Feng XIAO et al. [42] on Arctic sea ice thickness.

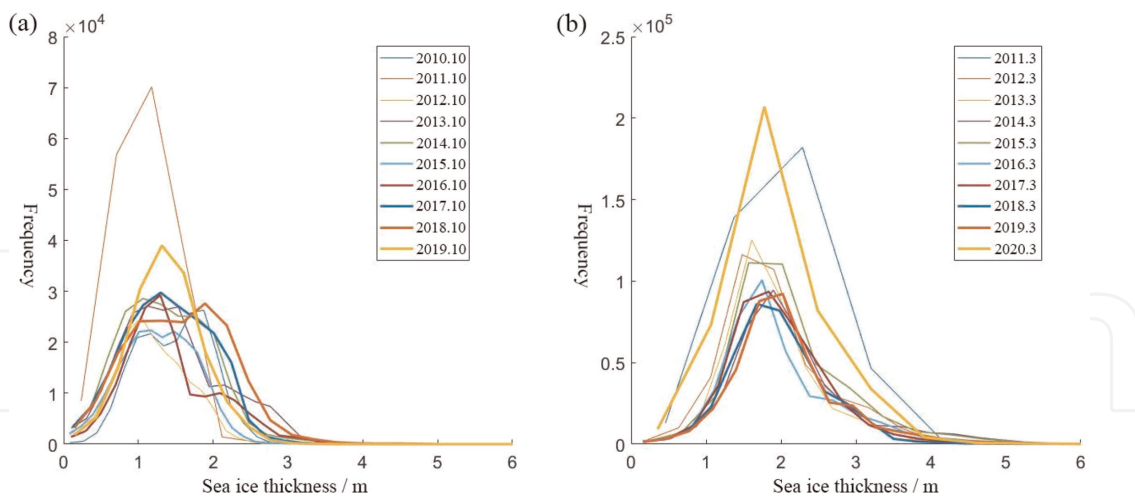


**Figure 16.**  
 Frequency and sea ice thickness in March and October from 2010 to 2020.

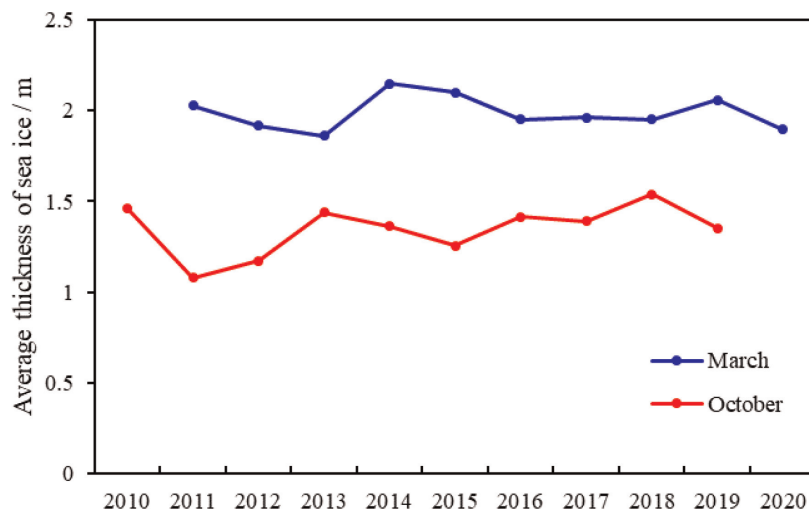


**Figure 17.**  
 The average thickness of sea ice in March and November from 2010 to 2020.

#### 4.2 Analysis of volume changes of first-year ice and multiyear ice

To further analyze the process and trend of sea ice change, the volume of first-year ice and multiyear ice was calculated separately over the years. **Figure 18** shows the variation of the sea ice volume in March from 2011 to 2020, and **Figure 19** shows the variation of the sea ice volume in October from 2010 to 2019.

There are small fluctuations in the total sea ice volume in March from 2011 to 2020, And from 2013 to 2014, the total sea ice volume increases by 10.41%. In addition, in 2020, the total sea ice volume decreases by 10.08%, and in the rest of the years, the volumes of the sea ice show some fluctuations with the variation rate being within 5%. Overall, the total volume of sea ice in the Arctic region was relatively stable in recent years. However, by analyzing the variations of the multi-year ice and the first-year ice volume, they appeared opposite trends in recent years. Multi-year ice volume increased by 61.93% in 2014 and 22.70% in 2017, while showing a continuous decreasing trend in 2018 and beyond. First-year ice volume decreased by 12.40% in 2014 and 12.51% in 2020, and increased by 15.53% in

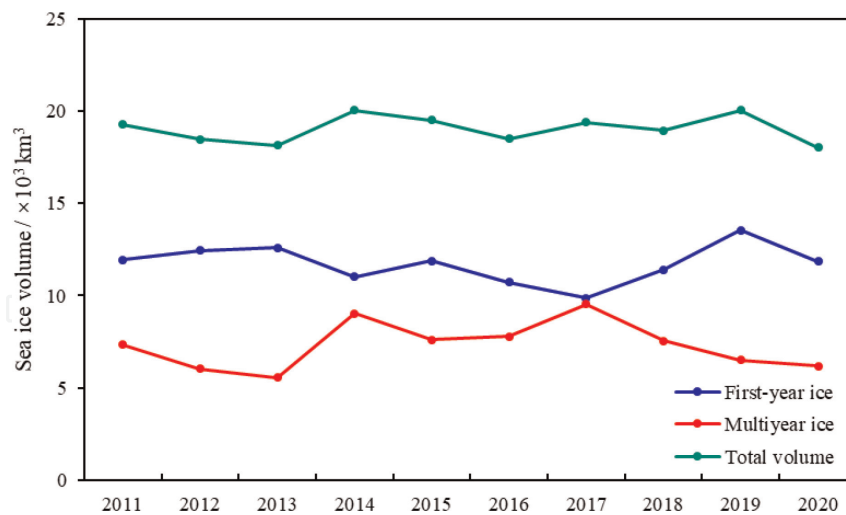


**Figure 18.**  
Folding line graph of sea ice volume change from March 2011 to 2020.

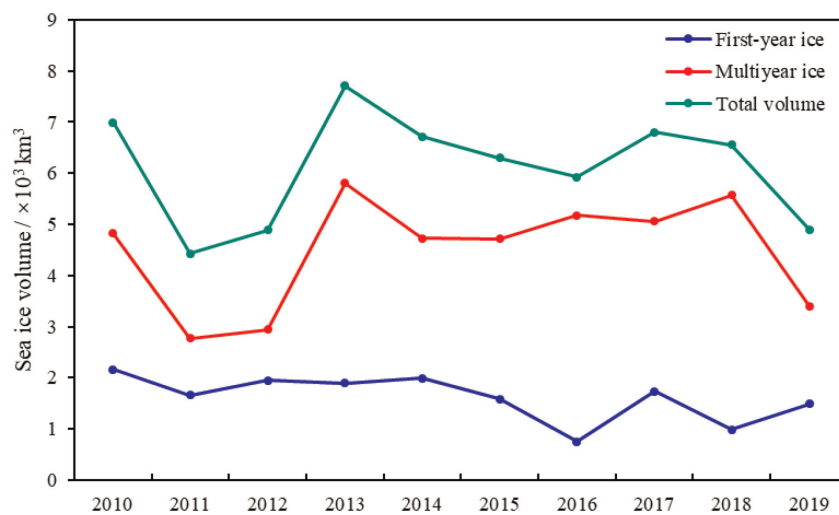


**Figure 19.**  
Folding line graph of sea ice volume change from October 2010 to 2019.

2018 and 18.85% in 2019. The volume changes of the first-year ice and the multi-year ice showed a negative correlation. The growth of one side was accompanied by the decrease of the other side.

From 2010 to 2019, the sea ice volume in October was highly variable. It decreased significantly in 2011 and showed a large increase in 2013. Furthermore, after 2017, the sea ice volume showed a continuous downward trend. Because usually, the life period of the first-year ice would not exist more than one summer, after the summer, the first-year ice maintains a very low total volume in October, and the volume variation of the multi-year ice would be consistent with the volume variation of the total sea ice. The first-year ice volume remained stable in 2014 and before. Except in 2017, the volume of the first-year ice increased to close to the pre-2014, it changed fluctuated less during the rest of the years. As shown in **Figure 18**, the first-year ice volume shows an increasing trend in March 2017. Overall, in recent years, the first-year ice in the Arctic region grew rapidly in winter and melted in summer, while the amount of the first-year ice which became the multi-year ice through the summer decreased.

In summary, from 2010 to 2019, the total volume of the sea ice in March over the years remained stable, which is consistent with the findings of Julienne Stroeve et al. [43]. The total volume of sea ice in October over the years fluctuates less after 2013, but the overall trend is gradually decreasing. However, the total multi-year ice volume showed a decreasing trend [44]. In winter, the increase of the total first-year ice hid the decrease of the total multi-year ice, and the change of the total sea ice volume was not obvious. While in the summer, much first-year ice melted, therefore the increase of the total first-year ice would be hard to compensate for the loss of the total multi-year ice.

## 5. Conclusion

In this study, the sea ice freeboard and thickness are calculated by the TFMRA algorithm based on the CryoSat-2 satellite L1b altimetry data in the ocean region north of 60°N latitude, including the echo signal preprocessing, waveform classification, and re-tracking correction. Furthermore, the thickness results were made into a grid of 5 km grid resolution and the average sea ice thickness and volume were calculated. From 2010 to 2020, the variation of the average sea ice thickness in March is relatively stable over the years. And there are small fluctuations in the average thickness change of the sea ice in October over the years, while the overall trend is stable. On the other hand, the total sea ice volume showed some small changes in recent years, while tends to decline slowly in general. The first-year ice shows a trend of increasing winter growth and summer ablation with a similar amount of growth and ablation. Decrease in the number of volumes of first-year ice transformed into multi-year ice. The total amount of the multi-year ice changed sharply in the previous years, while showing a slow decreasing trend in recent years.

Our results show that the errors are present in current estimations of Arctic sea ice thickness. Firstly, the threshold  $q$  used to calculate echoes is an empirical value, which might introduce some errors in a small range. Secondly, due to the limited amount of Cryosat-2 altimetry data available, the sea ice thickness inversion results exhibit some striped contamination, which may lead to errors. Furthermore, uncertainties arising from changes in snow thickness, sea ice density, snow density, seawater density values, and Arctic circulation patterns can impact the accuracy of sea ice thickness inversions to varying degrees.

Despite these uncertainties, the CryoSat-2 altimetry satellite method offers high accuracy and volume, making it a reliable tool for monitoring Arctic sea ice. In future research, we aim to further investigate the variability of Arctic sea ice thickness for a more comprehensive understanding of this important area.

## Conflict of interest

The authors declare no conflict of interest.

IntechOpen

## **Author details**

Xubing Zhang<sup>1</sup>, Ruizhi Li<sup>1</sup>, Wenxi Li<sup>1\*</sup>, Liang Zhang<sup>2</sup> and Kai Wang<sup>3</sup>

1 School of Geography and Information Engineering, China University of Geosciences, Wuhan, China


2 State Key Laboratory of Geological Processes and Mineral Resources, School of Earth Sciences, Planetary Science Institute, China University of Geosciences, Wuhan, China

3 School of Geophysics and Geomatics, China University of Geosciences, Wuhan, China

\*Address all correspondence to: [hmyu\\_fzdmxtfz@126.com](mailto:hmyu_fzdmxtfz@126.com)

## **IntechOpen**

---

© 2023 The Author(s). Licensee IntechOpen. This chapter is distributed under the terms of the Creative Commons Attribution License (<http://creativecommons.org/licenses/by/3.0>), which permits unrestricted use, distribution, and reproduction in any medium, provided the original work is properly cited. 

## References

- [1] Djepa V. Sensitivity analyses of sea ice thickness retrieval from radar altimeter. *Journal of Survival Mapping Engineering*. 2014;**2**:44-45
- [2] Bouzinac C. *CryoSat Product Handbook*: ESRIN/ESA and Mullard Space Science Laboratory. London, UK: University College London; 2013
- [3] Laxon S, Peacock N, Smith D. High interannual variability of sea ice thickness in the Arctic region. *Nature*. 2003;**425**(6961):947-950
- [4] Peacock NR, Laxon SW. Sea surface height determination in the Arctic Ocean from ERS altimetry. *Journal of Geophysical Research: Oceans*. 2004; **109**:C7. DOI: 10.1029/2001JC001026
- [5] Kwok R, Cunningham GF, Wensnahan M, Rigor I, Zwally HJ, Yi D. Thinning and volume loss of the Arctic Ocean sea ice cover: 2003–2008. *Journal of Geophysical Research: Oceans*. 2009; **114**(C7):1-16. DOI: 10.1029/2009jc005312
- [6] Laxon SW, Giles KA, Ridout AL, Wingham DJ, Willatt R, Cullen R, et al. CryoSat-2 estimates of Arctic Sea ice thickness and volume. *Geophysical Research Letters*. 2013;**40**(4):732-737. DOI: 10.1002/grl.50193
- [7] Rinne E, Similä M. Utilisation of CryoSat-2 SAR altimeter in operational ice charting. *The Cryosphere*. 2016; **10**(1):121-131. DOI: 10.5194/tc-10-121-2016
- [8] Lee S, Im J, Kim J, Kim M, Shin M, Kim H, et al. Arctic Sea ice thickness estimation from CryoSat-2 satellite data using machine learning-based lead detection. *Remote Sensing*. 2016;**8**(9): 698. DOI: 10.3390/rs8090698
- [9] Giles KA, Laxon SW, Wingham DJ, Wallis DW, Krabill WB, Leuschen CJ, et al. Combined airborne laser and radar altimeter measurements over the Fram Strait in May 2002. *Remote Sensing of Environment*. 2007;**111**(2–3):182-194. DOI: 10.1016/j.rse.2007.02.037
- [10] Jain M, Andersen OB, Dall J, Stenseng L. Sea surface height determination in the Arctic using Cryosat-2 SAR data from primary peak empirical retracers. *Advances in Space Research*. 2015;**55**(1):40-50. DOI: 10.1016/j.asr.2014.09.006
- [11] Helm V, Humbert A, Miller H. Elevation and elevation change of Greenland and Antarctica derived from CryoSat-2. *The Cryosphere*. 2014;**8**(4): 1539-1559. DOI: 10.5194/tc-8-1539-2014
- [12] Kurtz NT, Galin N, Studinger M. An improved CryoSat-2 sea ice freeboard retrieval algorithm through the use of waveform fitting. *The Cryosphere*. 2014; **8**:1217-1237. DOI: 10.5194/tc-8-1217-2014
- [13] Rostosky P, Spreen G, Farrell SL, Frost T, Heygster G, Melsheimer C. Snow depth retrieval on Arctic Sea ice from passive microwave radiometers—Improvements and extensions to multiyear ice using lower frequencies. *Journal of Geophysical Research: Oceans*. 2018;**123**(10):7120-7138. DOI: 10.1029/2018JC014028
- [14] Warren SG, Rigor IG, Untersteiner N, Vladimir R, Nikolay B, Yevgeniy A, et al. Snow depth on Arctic Sea ice. *Journal of Climate*. 1999;**12**(6): 1814-1829. DOI: 10.1175/1520-0442(1999)012<1814:SDOASI>2.0.CO;2
- [15] Kurtz NT, Farrell SL. Large-scale surveys of snow depth on Arctic Sea ice

from operation IceBridge. *Geophysical Research Letters*. 2011;**38**(20):1-5. DOI: 10.1029/2011GL049216

[16] Cavalieri D, Markus T, Comiso J. Amsr-e/Aqua Daily 13 12.5 Km Brightness Temperature, Sea Ice Concentration, and Snow Depth Polar Grids v002. Boulder, Colorado USA: National Snow and Ice Data Center; 2004. pp. 9017-9024

[17] Stroeve J, Meier W. *Sea Ice Trends and Climatologies from SMMR and SSM/I-SSMIS, Version 1*. Boulder, Colorado, USA: NASA National Snow and Ice Data Center Distributed Active Archive Center; 2003

[18] Fetterer F, Stewart JS, Meier WN. *MASAM2: Daily 4 Km Arctic Sea Ice Concentration, Version 1*. Boulder, CO: National Snow and Ice Data Center; 2015

[19] Aaboe S, Breivik L, Sørensen A. *Global Sea Ice Edge and Type Product user's Manual*. France: EUMETSAT OSISAF; 2016

[20] Brown RD, Brasnett B. Canadian Meteorological Centre (CMC) daily snow depth analysis data. *Environment Canada*. 2010;**169**:1-18

[21] Krabill WB. *IceBridge ATML1B Qfit Elevation and Return Strength*. Boulder, CO: NASA DAAC at the National Snow and Ice Data Center; 2010

[22] Kurtz N, Studinger MS, Harbeck J, Onana V, Farrell SL. *IceBridge Sea Ice Freeboard, Snow Depth, and Thickness, Version 1*. Boulder, CO: NASA National Snow and Ice Data Center Distributed Active Archive Center; 2012. DOI: 10.5067/7XJ9HRV50057

[23] Gaina C, Werner SC, Saltus R, Maus S. *Circum-Arctic mapping project*:

*New magnetic and gravity anomaly maps of the Arctic*. Geological Society. 2011;**35**(1):39-48. DOI: 10.1144/M35.3

[24] Skourup H, Farrell SL, Hendricks S, Ricker R, Armitage WK, Ridout A, et al. An assessment of state-of-the-art mean sea surface and geoid models of the Arctic Ocean: Implications for sea ice freeboard retrieval. *Journal of Geophysical Research: Oceans*. 2017; **122**(11):8593-8613. DOI: 10.1002/2017JC013176

[25] Ridout A. *New Mean Sea Surface for the CryoSat-2 L2 SAR Chain*. London, UK: UCL; 2014

[26] Feng S, Li F, Li S. *Introduction to Marine Science*. Beijing, China: Higher Education Press; 1999

[27] Guo J. *Satellite Radar Altimetry Waveform Redefinition and Application*. Beijing, China: Survey and Mapping Press; 2013

[28] Zhai G, Huang M, Ouyang Y, Lu X. *Satellite altimetry principles and their applications*. *Hydrographic Surveying and Charting*. 2002;**22**(1):57-62. DOI: 10.3969/j.issn.1671-3044.2002.01.016

[29] Laxon S. Sea ice altimeter processing scheme at the EODC. *International Journal of Remote Sensing*. 1994;**15**(4): 915-924. DOI: 10.1080/01431169408954124

[30] Thorpe SA. Fluid dynamics, introduction and laboratory experiments. In: *Encyclopedia of Ocean Sciences*. Cambridge, US: Academic Press; 2001. p. 1070. DOI: 10.1006/rwos.2001.0500

[31] Tilling RL, Ridout A, Shepherd A. Estimating Arctic Sea ice thickness and volume using CryoSat-2 radar altimeter

- data. *Advances in Space Research*. 2018; **62**(6):1203-1225. DOI: 10.1016/j.asr.2017.10.051
- [32] Spreen G, Kern S, Stammer D, Hansen E. Fram Strait sea ice volume export estimated between 2003 and 2008 from satellite data. *Geophysical Research Letters*. 2009;**36**(19):1-6. DOI: 10.1029/2009GL039591
- [33] Alexandrov V, Sandven S, Wahlin J, Johannessen OM. The relation between sea ice thickness and freeboard in the Arctic. *The Cryosphere*. 2010;**4**:373-380. DOI: 10.5194/tc-4-373-2010
- [34] Golden KM, Ackley SF, Lytle VI. The percolation phase transition in sea ice. *Science*. 1998;**282**(5397):2238-2241. DOI: science.282.5397.2238
- [35] Lytle VI, Ackley SF. Heat flux through sea ice in the western Weddell Sea: Convective and conductive transfer processes. *Journal of Geophysical Research: Oceans*. 1996;**101**(C4): 8853-8868. DOI: 10.1029/95JC03675
- [36] Shen S. A Study of CrvoSat-2 Based Sea Ice Thickness Inversion Method. *Research on Sea Ice Thickness Inversion Method Based on CrvoSat-2*. Nanjing: Nanjing University; 2018
- [37] Lewis MJ, Tison J, Weissling B, Delille B, Ackley SF, Brabant F, et al. Sea ice and snow cover characteristics during the winter-spring transition in the Bellingshausen Sea: An overview of SIMBA 2007. *Deep Sea Research Part II: Topical Studies in Oceanography*. 2011; **58**(9-10):1019-1038. DOI: 10.1016/j.dsr2.2010.10.027
- [38] Farrell SL, Kurtz N, Connor LN, Elder BC, Leuschen C, Leuschen C, et al. A first assessment of IceBridge snow and ice thickness data over Arctic Sea ice. *IEEE Transactions on Geoscience and Remote Sensing*. 2011;**50**(6):2098-2111. DOI: 10.1109/TGRS.2011.2170843
- [39] Jiao Y, You Q, Li Y, Zhou Y. Seasonal and interdecadal variability of Arctic Sea ice and temperature response in East Asia. In: 35th Annual Meeting of the Chinese Meteorological Society S7 East Asia Climate, Variability Mechanisms of Extreme Climate Events and Climate Prediction. Vol. 11. Beijing, China: Chinese Meteorological Society; 2018. p. 423
- [40] Kwok R, Rothrock DA. Decline in Arctic Sea ice thickness from submarine and ICESat records: 1958-2008. *Geophysical Research Letters*. 2009; **2009**:36. DOI: 10.1029/2009GL039035
- [41] Sumata H, de Steur L, Divine DV, et al. Regime shift in Arctic Ocean sea ice thickness. *Nature*. 2023;**615**(7952): 443-449. DOI: 10.1038/s41586-022-05686-x
- [42] Xiao F, Zhang S, Li J, et al. Arctic Sea ice thickness variations from CryoSat-2 satellite altimetry data. *Science China Earth Sciences*. 2021;**64**(7):1080-1089. DOI: 10.1007/s11430-020-9777-9
- [43] Stroeve J, Holland MM, Meier W, et al. Arctic Sea ice decline: Faster than forecast. *Geophysical research letters*. 2007;**34**(9). DOI: 10.1029/2007GL029703
- [44] Pörtner HO, Roberts DC, Masson-Delmotte V, et al. The Ocean and Cryosphere in A Changing Climate. IPCC Special Report on The Ocean and Cryosphere in a Changing Climate 2019. p. 1155. DOI: 10.1017/9781009157964